

Chapter 23

Characterisation of the Deformation and Fracture Behaviour of Elastomers Under Biaxial Deformation

K. Schneider, R. Calabrò, R. Lombardi, C. Kipscholl, T. Horst,
A. Schulze, S. Dedova and G. Heinrich

Abstract A new biaxial testing machine from COESFELD is presented, which enables essential new and more comprehensive opportunities for non-destructive and fracture mechanical testing of elastomers, mainly under dynamical load. Some possible applications are described in detail.

23.1 Introduction

Elastomers are a widely used group of materials, which are used under very different loading conditions. For an appropriate use of these materials it is necessary to model devices under application oriented conditions. Therefore besides the straightforward quasi-static and dynamic unidirectional tensile, compression and

K. Schneider (✉) · R. Lombardi · A. Schulze · S. Dedova · G. Heinrich
Leibniz Institute for Polymer Research Dresden e.V., Dresden, Germany

R. Calabrò
Department of Chemistry, Materials and Chemical Engineering,
Polytechnic University of Milan, Milan, Italy

R. Lombardi
University of Naples Federico II, Naples, Italy

C. Kipscholl
Coesfeld GmbH & Co. KG, Dortmund, Germany

S. Dedova · G. Heinrich
Dresden University of Technology, Dresden, Germany

T. Horst
Faculty of Automobile and Mechanical Engineering, University of Applied Sciences
Zwickau, Zwickau, Germany

A. Schulze
Chemnitz University of Technology, Chemnitz, Germany

R. Lombardi
Bridgestone Technical Center Europe, Rome, Italy

shear tests with the material also tests under well-defined biaxial load are essential. As well for the characterisation of the failure behaviour of elastomers besides the classical uniaxial Tear Fatigue Test also investigations under complex application-related load are preferable. In cooperation between Coesfeld GmbH & Co. KG Dortmund and the Leibniz-Institut für Polymerforschung Dresden (IPF) a Biax Tester was designed, built and checked [1–3]. This new biaxial testing machine enables essential new and more comprehensive opportunities for non-destructive and fracture mechanical testing of elastomers, mainly under dynamical load. The device and some first results shall be presented here in detail.

23.2 Concept of the Biaxial Test Stand

An outline of the Biax Tester for Elastomer Materials is shown in Fig. 23.1. It consists mainly of four separately driven electro-mechanical linear motors, each with load cell and displacement sensor as well as a clamping system, which are arranged paired on opposite sites and have each a displacement range of initially 30 mm. By certain enhancement of the clamping system in the meantime the displacement of each axis could be increased to 120 mm.

The motors are controlled separately; they can transfer different deformation (overall load configurations) to the sample. The loads were defined via displacement profiles and are freely configurable (e.g. sine wave, pulse, rectangle, triangle

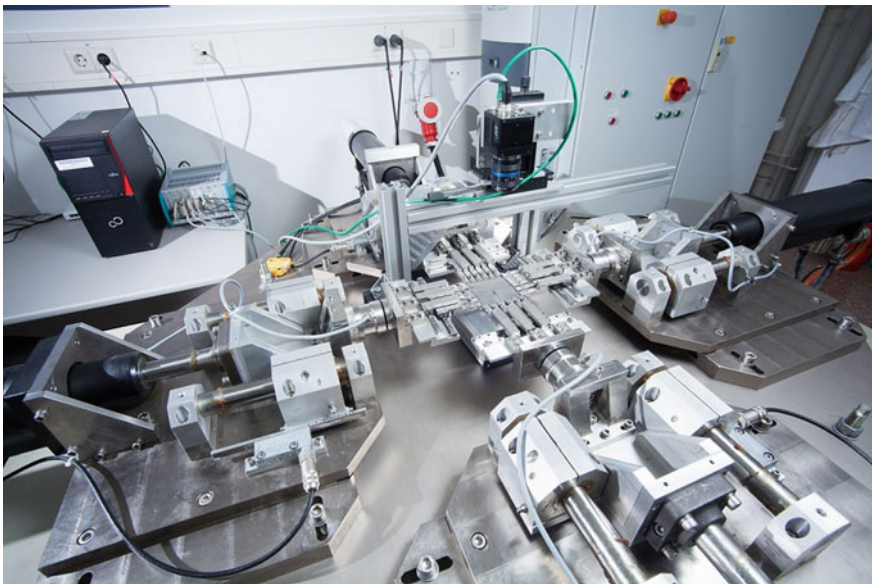


Fig. 23.1 Biax Test Stand of Coesfeld GmbH & Co. KG

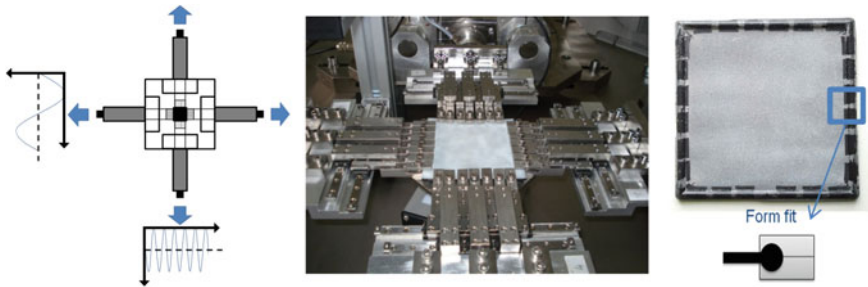


Fig. 23.2 Sketch of the test stand with individually configurable displacement profiles for each axis (*left*); clamping system of the Biax Tester, here with 7 individual clamps per axis (*middle*), principle of clamping by form fit (*right*)

or also free definable as external file). The real clamp displacement is always monitored by a displacement sensor. For the preferable dynamic tests each motor has an adaptive controller which realises the desired deformation profile. After a few cycles an optimal target performance is realised. Each linear motor is equipped with a load cell which is insensitive with respect to transversal load. The load cells carry directly the clamping system.

Each clamping system consists of a rail with up to 10 individual clamps with a width of each 10 mm, which can slide by a wheel bearing transversal to the loading axis, see Fig. 23.2.

In the case of clamps with traction the local load of the clamps causes irreproducible deformations. Therefore here preferable clamps with form fit are used and the rectangular (or squared) samples of 1–2 mm thickness should have a cylindrical edge with a diameter of 4 mm, which fits the clamp, see Fig. 23.2, right side. To prevent undefined displacements at the vertices the external clamps of each rail can be connected with each other.

A good adjustment of the motors is necessary to prevent friction and transversal load at the clamps. During measurement with frequencies above 10 Hz it is necessary to have the inertia of the clamps in mind to correct the monitored load (Table 23.1).

Mainly for the investigation of heterogeneous stress stages, like e.g. in samples with a crack, it is necessary to capture the 2D strain stage of the sample by image processing techniques. This is possible following the deformation of a random pattern at the sample surface and evaluation e.g. by ARAMIS (Digital Image Correlation (DIC), Fa. GOM, Braunschweig, Germany), or by recording of the crack contour at homogeneous illumination of the sample of the bottom side (Digital Image Elaboration (DIE)). For these tasks an infrared (IR) camera is used, which can be mounted feely on the ground plate by magnetic bases. The illumination of the sample is realised from top or bottom side, see Fig. 23.3.

The camera can be adapted for the different tasks, especially recording the whole sample as well as of individual details of the sample each with optimal resolution.

Table 23.1 Specifications of the Biax Test Stand

Excitation	Each axis separately or also pair-wise parallel feed
Displacement profiles	Sine wave, Gauss pulse, triangle, rectangle, free defined by the user
Load speed	Maximum 50 Hz, practically 10 Hz, maximum displacement each up to 30 mm (meanwhile improved to 60 mm)
Load range	2000 N
Data acquisition	Whole cycles, individual cycles or individual parameters of the cycles
Image acquisition	Continuous or triggered by individual events
Sample size	Rectangular or squared with up to $100 \times 100 \text{ mm}^2$, preferable $85 \times 85 \text{ mm}^2$ with circumferential cylindrical bulge with a diameter of 4 mm

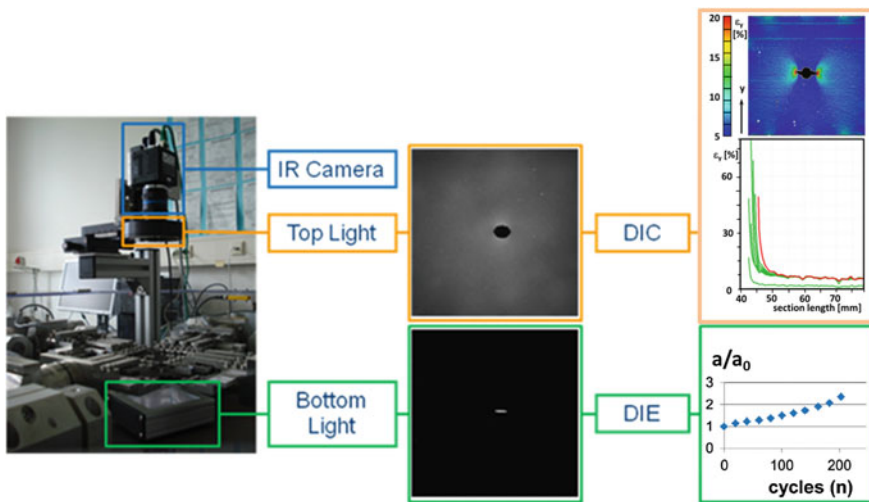


Fig. 23.3 Concept of the image acquisition system at the Biax Test Stand: experimental arrangement (*left*), captured images (*middle*), estimated diagrams: strain transversal to the crack direction versus the distance to the crack tip and 2D strain field (*right side, top*), increase of the crack length versus the number of loading cycles (*right side, bottom*)

23.3 Upgrading of a Biaxial Testing Method

The initial clamping system has some limits for the performance of experiments. These are mainly the restriction of the maximum length of stroke for each side (60 mm or 77% deformation for each axis) and the weight of the moving parts. The last one allows working with high deformation only with relative low frequencies due to the high inertial force.

For this reason the new clamping system was designed and built. The important points were:

- Increase of biaxial deformation range up to 150%,
- Possibility to test materials at higher frequencies,
- Possibility of making the crack propagation tests (relatively large specimen),
- Provide the homogeneous deformation field (for the error-free local deformation field analysis).

23.3.1 New Clamping System for High Biaxial Deformation

The new clamping system is shown on the Fig. 23.4. The new design of the clamp rails allows the measurement up to 150% biaxial deformation. This possibility is really important for such experiments like the parameterisation of constitutive models.

The new concept includes the weight reduction. New system is made of a carbon fibre composite and reaches much lower weight while retaining the same stiffness of the system.

The new system was tested under harmonic loading and compared with the old one. For this reason the layout parameters of Biaxial Test Stand were used. Due to the constructing changes and weight reduction the new design enables a much higher amplitude–frequency working range, compared with the old system (see Fig. 23.4 left).

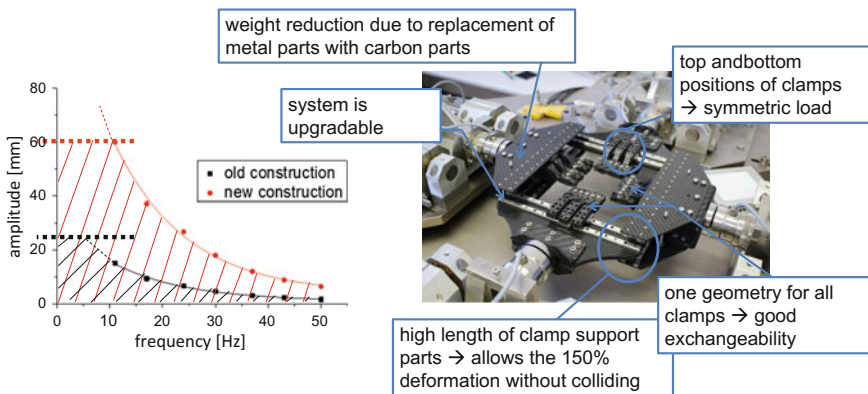


Fig. 23.4 New clamping system (*right*) and the possible amplitude–frequency working range (*left*)

23.3.2 Specimen Geometry

During the previous experiments some inhomogeneities in the deformation field, especially in the near-clamps area, were detected. This effect rises with a growing strain. It leads to errors in the strain field analysis which is necessary for example for the J -integral. Before the improvement of the new specimen geometry, the different concepts, used for different materials, were analysed.

Some biaxial specimens for rubber are known from the literature [4, 5]. The both concepts provide biaxial conditions in the middle of the specimen. It allows measuring the stress–strain behaviour, but cannot be used for the crack propagation experiments. For another materials (for example metals) some another geometries are used [6–12]. Using some of such concepts the crack grow experiments are possible. However, the specimen geometries in these cases cannot be used for the high strains. Some of the concept shows the increase of homogeneity by reduction of the middle thickness of the specimen. This idea was adopted and analysed for the current specimen geometry of Biax Test Stand.

The new geometry consists of two thicknesses of the plate—the middle area has a thickness of 1.5 mm and the border area with a thickness of 3 mm and width of 7 mm. At the edge there is again the cylindrical bulge for the form-fit. Figure 23.5 shows the FEM simulation of the deformation field of the two specimen geometries—currently used geometry and a new concept. The simulation was made using ANSYS software and Ogden model 3th order for a rubber material from [13]. For the simulation one quarter of the specimen was used.

The same state of applied residual strain leads to a different distribution of local strain over the sample. The deformed area of the previous sample shows a higher inhomogeneity compared with the new one. The inhomogeneous range has a width of about 20 mm from each specimen edge. With a stretched size of 158 mm this is equivalent to about 25% of the length (for each axis). In the middle area of the specimen there are no such distinct strain differences.

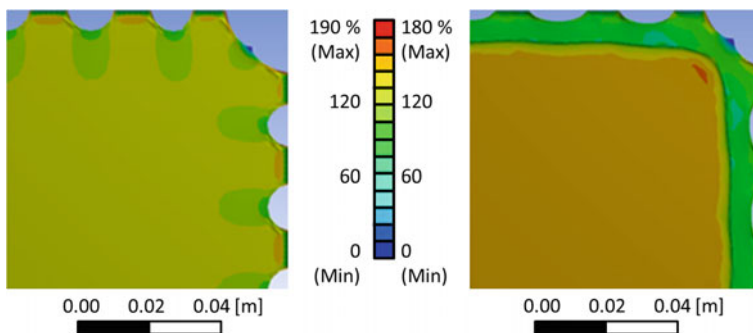


Fig. 23.5 FE analysis of elastic equivalent strain for the current specimen geometry (*left*) and new specimen geometry (*right*) ($\Delta\varepsilon = 100\%$)

The new specimen geometry ensures a high homogeneity of the biaxial strain in the middle area. The effect of local clamp inhomogeneities becomes compensated in the thicker edge area. This area corresponds to about 9% of the stretched specimen length.

23.3.3 Crack Propagation with the New Specimen

The improvements of the new geometry for the crack propagation experiments was analysed by FEM simulation and compared with the measured results. For this reason a notched sample (notch length of 30 mm) was used and stretched up to 48 mm in the y-direction. After that the strain field was analysed with the ARAMIS system (Fig. 23.6a).

The same experiment was repeated for the current and new geometry using FE simulation (Fig. 23.6b, c).

The measured and simulated current geometry shows a good agreement of results (Fig. 23.6a, b). The thick edge region of a new specimen remains inviolated and has no effect on the crack tip. That means that the new specimen can be used for the crack propagation experiments in the same way like a current geometry.

23.4 Material

Some representative tests were performed using natural rubber (NR), solution styrene-butadiene rubber (SBR) and hydrated acrylonitrile-butadiene rubber (HNBR) with carbon black (CB) as filler. Composition and labeling are shown in Table 23.2. Squared samples with a lateral length of 85 mm and a circumferential bulge of 4 mm were vulcanised in the IPF.

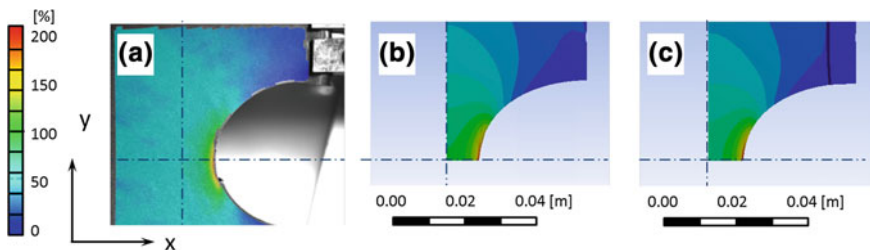
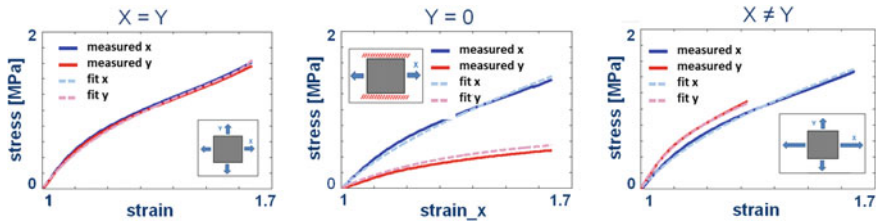


Fig. 23.6 FE analysis of equivalent strain for current and new geometry ($\varepsilon_x = 0$; $\varepsilon_y = 62\%$): **a** measured specimen, **b** current geometry (simulation), **c** new geometry (simulation)

Table 23.2 Materials

Labeling	Matrix	Filler
NR/50phrCB	Natural rubber	50 phr CB N550
SBR/50phrCB	Solution styrene–butadiene rubber	50 phr CB N550
HNBR/30phrCB	Hydrated acrylonitrile–butadiene rubber	30 phr CB N339

**Fig. 23.7** Stress–strain behaviour under different load, measured values and values fitted by the extended tube model

23.5 Results

23.5.1 Material Behaviour Under Biaxial Load

The Biax Tester enables the estimation of stress–strain behaviour under complex load, e.g. the ratio of the x- and y-strain can be chosen free. Afterwards the different tests can be fitted by a suitable model, e.g. the extended tube model, see Fig. 23.7.

Like in the uniaxial case the characterisation of the stress–strain behaviour under biaxial load shows differences in loading and unloading curves (Fig. 23.8). Comparing both curves it is possible to split the total energy W_t into elastically stored and dissipated energy resp. W_e and W_d according to

$$W_d = W_t - W_e = \int_{\varepsilon_r(\text{loading})}^{\varepsilon_{\max}} \sigma_{\text{loading}} d\varepsilon - \int_{\varepsilon_r(\text{unloading})}^{\varepsilon_{\max}} \sigma_{\text{unloading}} d\varepsilon. \quad (23.1)$$

Here ε_r is the strain in the unloaded state during loading and unloading step, ε_{\max} the maximal strain; σ_{loading} resp. $\sigma_{\text{unloading}}$ are the stresses during the loading and unloading step.

As example a set of biaxial tests was performed with CB-filled natural rubber NR/50phrCB and strains ε_1 and ε_2 resp. in the range of 0–35% at 1 Hz. Pre-conditioning was performed by 500 cycles at maximum displacement. The measurement of the force–displacement diagrams was performed always after 100 cycles at the nominal strain, see Fig. 23.9.

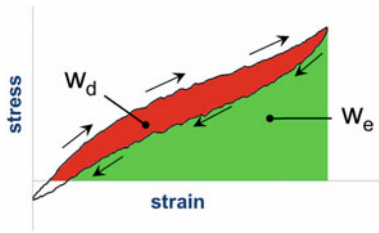
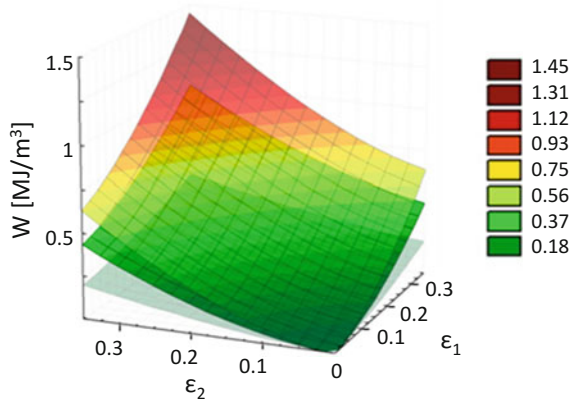


Fig. 23.8 Separation of the performed work to elastically stored and dissipated energy

Fig. 23.9 Total energy (upper surface), elastically stored energy (median surface) and dissipated energy (bottom surface) via strain at biaxial load of NR/50phrCB



In the range under investigation the elastically stored energy compared with the total applied energy is in the range of $W_e/W_t = 0.6-0.7$, while the dissipated amount is at $W_d/W_t = 0.3-0.4$. Thereby the amount of dissipated energy decreases slightly with increasing strain. The investigations will be continued within a larger strain range to check the parameterisation of material laws for bulk modelling.

23.5.2 Strain Amplification at the Crack Tip of a SENT Sample

By digital image correlation it is possible to estimate strain fields of 2D sample. So it is also possible to get strain amplification in the ligament of a SENT specimen (single-edge-notched tensile sample). In Fig. 23.10a certain strain step of a filled natural rubber sample NR/50phrCB is shown. Because the strain amplification is dependent on the sharpness of the pre-notch, the tip of the initial crack of 6 mm was sharpened by a razor blade.

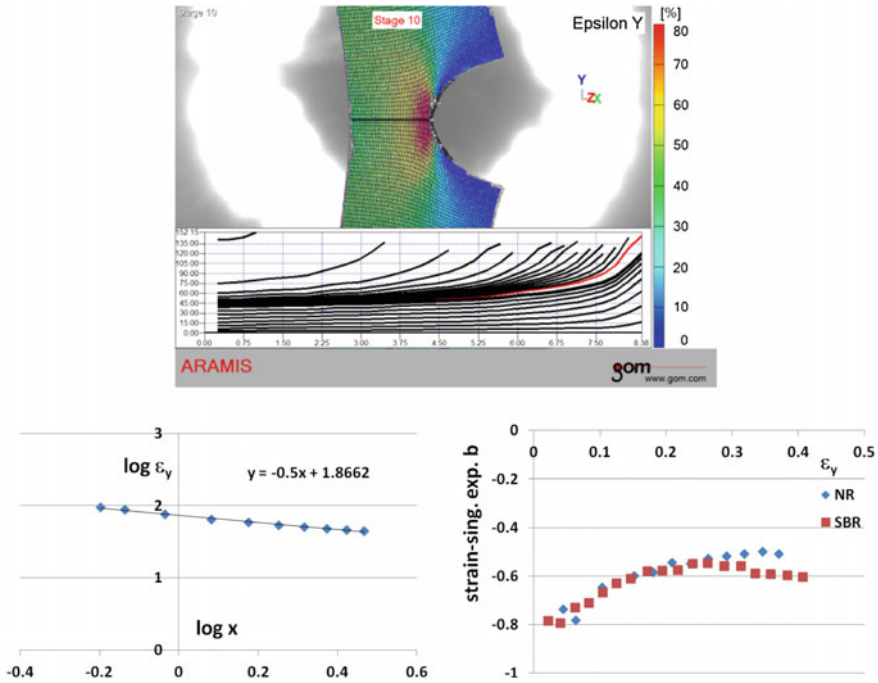


Fig. 23.10 Strain field around the crack tip of a SENT sample (*top*), estimation of the exponent of the strain singularity by linear regression of the strain versus the distance to the crack tip on a log-scale for NR/50phrCB (*bottom left*) as well as dependence of the exponent of strain singularity from the external applied strain for NR/50phrCB and SBR/50phrCB (*bottom right*)

The strain transversal to the crack propagation ϵ_y can be approximated by a power law as

$$\epsilon_y = kx^b. \tag{23.2}$$

Here b is the exponent of the strain singularity, k a pre-exponential factor. It should have the value of -0.5 [14]. In Fig. 23.10 the procedure for the estimation of b is illustrated and the exponents of two different materials are shown.

23.5.3 Crack Propagation Under Biaxial Load

Figure 23.11 shows an example of stable crack propagation. A centered pre-crack in the sample (Griffith crack, initial length 6 mm, crack tips sharpened by a razor blade) propagates under cyclic loading with amplitudes of $\epsilon_y = 25\%$ transversal to the crack and $\epsilon_x = 45\%$ in crack direction initially stable before spontaneous failure happens.

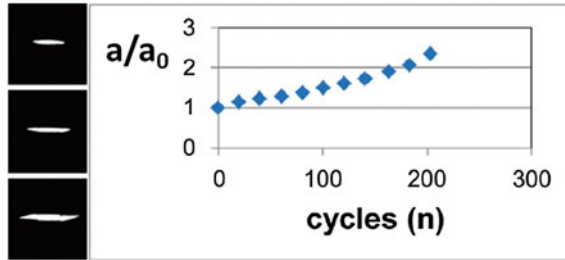


Fig. 23.11 Propagating crack after 0, 80 and 160 cycles respectively (*left side*) and change in the crack length a with the number of cycles, divided by the initial crack length a_0 ; harmonic loading of filled natural rubber NR/50phrCB during stable crack propagation at 1 Hz and strain amplitude $\varepsilon_y = 25\%$ in transversal direction (*crack opening*), $\varepsilon_x = 45\%$ in crack direction (*horizontally*)

23.5.4 Crack Propagation and Estimation of the Tearing Energy

Fracture mechanical characterisation of elastomers is possible by the concept of tearing energy, introduced by Rivlin and Thomas [15]. The tearing energy is the energy, which is necessary to increase the fracture surface by an infinitesimal amount. It can be estimated via the loss of elastically stored energy during infinitesimal crack propagation as

$$T = - \left. \frac{dW}{h_0 da} \right|_{l=\text{const.}} \quad (23.3)$$

Here W is the strain energy, h_0 the sample thickness and da the increment of the crack length. The differentiation dW/da has to be performed with constant displacement l of the boundaries. The work of external forces is zero.

For practical applications the tear fatigue test for rubber is established. Here a narrow specimen with a lateral pre-crack is loaded cyclically and the crack propagation is monitored. This test recently was modified in that way, that also pure-shear specimens with pre-crack can be used. Those specimen allow a more reliable estimation of the tearing energy [16, 17].

The evaluation of the measurements will be performed in analogy to the classical pure-shear test. The propagation of the crack on both sides of the homogeneous stretched resp. failed sample is monitored; the ratio of both values is estimated. Both evaluations were performed on the basis of the expressions for the estimation of the tearing energy in the case of self-similar crack propagation [15]. Numerous tests showed that the initial crack under biaxial load often becomes deflected yet in the first stage of crack propagation. Therefore the classical evaluation is not possible in these cases.

An alternative fracture mechanical characterisation can be performed using a hybrid method. The mean idea is that the hyper-elastic behaviour of the elastomers

can be characterised by certain parameters of an appropriate material model, which is parameterised by a set of different homogeneous deformation states. In the present case the Ogden model [18] as well as the extended tube model of rubber elasticity [19, 20] were used successfully. After the estimation of the deformation fields of the notched sample, using the material model, the elastic energy density is estimated and by this the related stress fields within the sample.

Generally there are two opportunities to estimate the tearing energy: On the one hand the direct evaluation of the elastically stored energy in the sample and its difference between two subsequent states with a small difference in the crack length, on the other hand the estimation of the J -integral [21], performing a line integral around the crack tip. Both methods are not restricted to self-similar crack propagation but also valid in the case of crack deflection. Therefore they are especially suitable for the use at the Biax Tester.

In the following the utilization of the J -integral shall be demonstrated. Here it is advantageous to use an integration path far away from the crack tip. This avoids experimental uncertainties in the estimation of the strain in regions of high displacement gradients in the direct vicinity of the crack. A vectorial form of the J -integral for large deformations will be evaluated [22–24] as

$$J = \int_{\Gamma} [\mathbf{W}^* \mathbf{I} - \mathbf{F}^T \mathbf{P}] \mathbf{n} \, d\Gamma. \quad (23.4)$$

Here \mathbf{W}^* is the elastic energy density, \mathbf{I} the unit vector, \mathbf{F} the deformation gradient, \mathbf{P} the 1st Piola-Kirchhoff stress tensor and \mathbf{n} the normal vector during the integration along a path Γ around the crack tip. In the case of hyperelasticity the stress \mathbf{P} can be written as

$$\mathbf{P} = \frac{\partial \mathbf{W}^*}{\partial \mathbf{F}} \quad (23.5)$$

(\mathbf{W}^* —elastic energy density, \mathbf{F} —deformation).

The components of the J -integral vector parallel to the tangent of the crack contour at the crack tip can be interpreted fracture mechanically as tearing energy [25, 26].

The applicability of this method was shown in the case of a pre-cracked squared sample under pure shear load (strain in crack direction was prevented). The values of the J -integral were compared with the values, estimated by the formula of Rivlin and Thomas for the estimation of the tearing energy for such a specimen

$$T = W^* h_0, \quad (23.6)$$

with the thickness h_0 of the specimen.

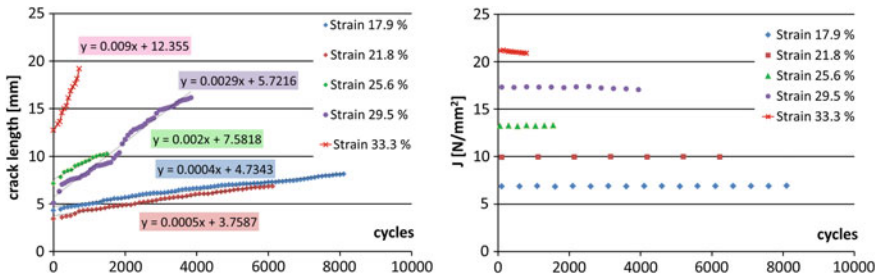


Fig. 23.12 Crack length versus the number of cycles, estimated at a hydrated acrylonitrile–butadiene rubber HNBR/30phrCB, with a sample under pure shear load (*left*) as well as tearing energy, estimated by the *J*-integral concept at different external load (*right*)

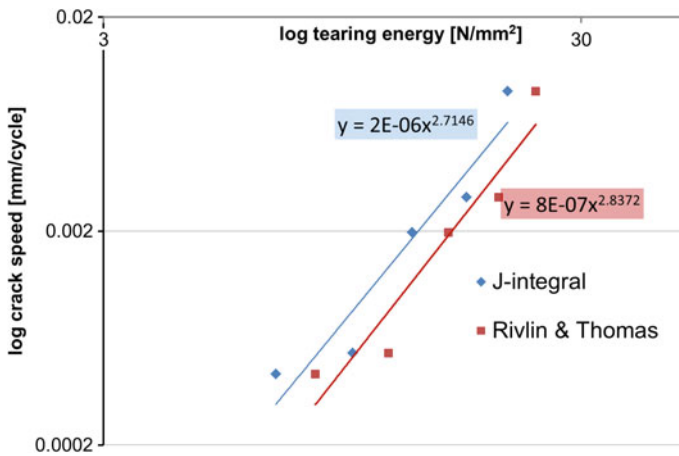


Fig. 23.13 Paris plot for a hydrated acrylonitrile–butadiene rubber (HNBR/30phrCB), estimated by the *J*-integral method as well as the method of Rivlin and Thomas, based on measurements of the Biax Tester

The measurements were performed at a hydrated acrylonitrile–butadiene rubber HNBR/30phrCB at squared samples by fixing the sample in crack direction and uniaxial load in transversal direction. Like in the case of the classical pure-shear specimen a constant crack propagation speed can be found, see Fig. 23.12.

In the Paris plot the tearing energies are shown, estimated with respect to the Rivlin-and-Thomas-method as well as the *J*-integral concept which allow conclusions about crack resistance of the samples. The small systematic differences are caused by dissipative processes within the bulk material, because the condition of hyperelasticity is not fulfilled sufficiently; see Fig. 23.13.

23.6 Conclusion

The new Biax Test Stand of Coesfeld strongly extends the static as well as dynamic characterisation techniques of elastomers. It delivers parameters for constitutive materials modelling under complex load, but also enables to trail the crack propagation under static as well as dynamic load, like it was shown at several examples. For a practice-oriented modelling of elastomer components also a quite complex characterisation is inevitable.

References

1. Biax Tester for Elastomer Material: Information brochure of Coesfeld GmbH & Co. KG., http://products.coesfeld.com/WebRoot/WAZ/Shops/44402782/5238/4E9A/BB18/5A3B/993E/D472/521A/76A8/61-490_Biastester_engl.pdf (01.06.2017)
2. Schneider, K., Calabrò, R., Lombardi, R., Kipscholl, C., Horst, T., Schulze, A., Heinrich, G.: Charakterisierung und Versagensverhalten von Elastomeren bei dynamischer biaxialer Belastung. *KGK–Kautsch. Gummi Kunstst.* **67**, 48–52 (2014)
3. Heinrich, G., Schneider, K., Calabrò, R., Lombardi, R., Kipscholl, C., Horst, T., Schulze, A., Gorelova, S.: Fracture behaviour of elastomers under dynamic biaxial loading conditions. *Tire Technol. Int.* 35–37 (2014)
4. Duncan, B.C.: Test Methods for Determining Hyperelastic Properties of Flexible Adhesives. NPL Report CMMT(MN)054, National Physical Laboratory, Teddington (1999)
5. Physical Testing Service: Information brochure of Axel Products Inc., <http://www.axelproducts.com> (01.06.2017)
6. Müller, W., Pöhlant, K.: New experiments for determining yield loci of sheet metal. *J. Mater. Process. Technol.* **60**, 643–648 (1996)
7. Kuwabara, T., Kuroda, K., Tvergaard, V., Nomura, K.: Use of abrupt strain path change for determining subsequent yield surface: Experimental study with metal sheets. *Acta Materialia*, 2071–2079 (2000)
8. Gozzi, J., Olsson, A., Lagerqvist, O.: Experimental investigation of the behavior of extra high strength steel. *Soc. Exp. Mech.* **45**, 533–540 (2005)
9. Yu, Y., Wan, M., Wu, X., Zhou, X.: Design of a cruciform biaxial tensile specimen for limit strain analysis by FEM. *J. Mater. Process. Technol.* **123**, 67–70 (2002)
10. Kelly, D.: Problems in creep testing under biaxial stress systems. *J. Strain Anal. Eng. Des.* **11**, 1–6 (1976)
11. Demmerle, S., Boehler, J.: Optimal design of biaxial tensile cruciform specimens. *J. Mech. Phys. Solids* **41**, 143–181 (1993)
12. Quak, G.: Biaxial testing of sheet metal: an experimental–numerical analysis. Master thesis, Eindhoven University of Technology, Eindhoven (2008)
13. Treloar, L.R.G.: Stress strain data for vulcanized rubber under various types of deformation. *Trans. Faraday Soc.* **40**, 59–70 (1944)
14. Broek, D.: Elementary Engineering Fracture Mechanics. Martinus Nijhoff Publishers, Dordrecht (1986)
15. Rivlin, R.S., Thomas, A.G.: Rupture of rubber. I. Characteristic energy of tearing. *J. Polym. Sci.* **10**, 291–318 (1953)
16. Stoček, R., Heinrich, G., Gehde, M., Kipscholl, R.: Analysis of dynamic crack propagation in elastomers by simultaneous tensile- and pure-shear-mode testing. In: Grellmann, W., Heinrich, G., Kaliske, M., Klüppel, M., Schneider, K., Vilgis, T.A. (eds.) *Fracture Mechanics*

- and Statistical Mechanics of Reinforced Elastomeric Blends. Springer, Berlin (2013), pp. 269–301
17. Stoček, R.: Dynamische Rissausbreitung in Elastomerwerkstoffen. PhD thesis, Technische Universität Chemnitz, Chemnitz (2012)
 18. Ogden, R.W.: Non-linear Elastic Deformation. Dover Publications, Mineola New York (1984)
 19. Kaliske, M., Heinrich, G.: An extended tube-model for rubber elasticity: Statistical-mechanical theory and finite element implementation. *Rubber Chem. Technol.* **72**, 602–632 (1999)
 20. Klüppel, M., Schramm, J.A.: Generalized tube model of rubber elasticity and stress softening of filler reinforced elastomer systems. *Macromol. Theory Simul.* **9**, 742–754 (2000)
 21. Rice, J.R., Rosengren, G.F.: Plane strain deformation near a crack in a power law hardening material. *J. Mech. Phys. Solids* **16**, 1–12 (1968)
 22. Maugin, G.A.: Material Inhomogeneities in Elasticity. Applied Mathematics and Mathematical Computation, Vol. 3. Chapman & Hall/CRC, Boca Raton (1993)
 23. Maugin, G.A., Muschik, W.: Thermodynamics with internal variables. Part I. General concepts; Part II. Applications. *J. Non-Equilib. Thermodyn.* **19**, 217–249, 250–289 (1994)
 24. Maugin, G.: Material forces: concepts and applications. *Appl. Mech. Rev.* **48**, 213–245 (1995)
 25. Behnke, R., Dal, H., Geißler, G., Näser, B., Netzker, C., Kaliske, M.: Macroscopical modeling and numerical simulation for the characterization of crack and durability properties of particle-reinforced elastomers. In: Grellmann, W., Heinrich, G., Kaliske, M., Klüppel, M., Schneider, K., Vilgis, T.A. (eds.) *Fracture Mechanics and Statistical Mechanics of Reinforced Elastomeric Blends*, pp. 167–226. Springer, Berlin (2013)
 26. Schulze, A.: Analyse der Verzerrungsfelder gekerbter Elastomerproben unter ein- und zweiachsiger äußerer Belastung. Diploma thesis, Technische Universität Chemnitz, Chemnitz (2012), 269–301